Aryne cycloaddition reaction as a facile and mild modification method for design of electrode materials for high-performance symmetric supercapacitor

Elizaveta Sviridova, Min Li, Alexandre Barras, Ahmed Addad, Mekhman Yusubov, Viktor Zhdankin, Akira Yoshimura, Sabine Szunerits, Pavel Postnikov, Rabah Boukherroub

Version of Record: https://www.sciencedirect.com/science/article/pii/S0013468620320600
Manuscript_32df73d54ce3abb5f70b5ed64b196fb8

Aryne cycloaddition reaction as a facile and mild modification method for design of electrode materials for high-performance symmetric supercapacitor

Elizaveta Sviridova[‡ 1], Min Li[‡ 2], Alexandre Barras[2], Ahmed Addad[3], Mekhman S. Yusubov[1], Viktor V. Zhdankin[4], Akira Yoshimura[1], Sabine Szunerits[2], Pavel S. Postnikov[1, 5*], Rabah Boukherroub[2*]

1. Research School of Chemistry and Applied Biomedical Sciences, Tomsk Polytechnic University, 634050 Tomsk, Russian Federation

2. Univ. Lille, CNRS, Centrale Lille, Univ. Polytechnique Hauts-de-France, IEMN, UMR CNRS 8520, F-59000 Lille, France

3. Univ. Lille, CNRS, UMR 8207 – UMET, F-59000 Lille, France

4. Department of Chemistry and Biochemistry, University of Minnesota, Duluth, MN 55812, USA

5. Department of Solid-State Engineering, University of Chemistry and Technology, 16628 Prague, Czech Republic

‡ Equal contributors

To whom correspondence should be addressed: Pavel Postnikov (postnikov@tpu.ru); Rabah Boukherroub (rabah.boukherroub@univ-lille.fr)

Abstract

Covalent modification of graphene-based materials can be considered as one of the most promising methods for tailoring their electrochemical properties and extending their application as electrode materials for supercapacitors. In this contribution, we report a facile and mild approach for the covalent functionalization of reduced graphene oxide (rGO) *via* aryne cycloaddition using pseudocyclic iodoxoborole as an aryne source. The structure and chemical composition of the functionalized rGO (f-rGO) were assessed by Fourier transform infrared (FTIR) spectroscopy, thermogravimetric analysis (TGA), ultraviolet–visible (UV-vis) absorption spectrophotometry, Raman spectroscopy and X-ray photoelectron spectroscopy (XPS), which revealed the negligible influence of covalent modification on the rGO structure. Transmission electron microscopy (TEM) imaging showed an increase of the interlayer distance from 0.38 to 0.46 nm upon functionalization. The electrochemical performance of f-rGO material was studied by cyclic voltammetry (CV), galvanostatic charge-discharge (GCD) and electrochemical impedance spectroscopy (EIS) techniques in 2 M KOH aqueous solution as the electrolyte. Under optimized conditions, the f-rGO displayed a high specific capacitance of 297 F g^{-1} at a current density of 1 A g^{-1}, which is much higher than that of unmodified rGO (170 F g^{-1} at 1 A g^{-1}). Therefore, the f-rGO was used to construct a symmetric supercapacitor device, exhibiting an energy density of 6.7 Wh kg^{-1} at a power density of 685.8 W kg^{-1}. The device exhibited good cycling stability and ability to maintain about 96% of the initial capacitance value after 10,000 cycles. The results obtained in the present study highlight the importance of graphene functionalization as an effective route to fabricate rGO-based materials with enhanced properties in energy storage devices.

Keywords: *reduced graphene oxide; iodonium salts; aryne cycloaddition reaction; covalent functionalization; symmetric supercapacitor.*

1. Introduction

Supercapacitors have aroused great attention as energy storage devices due to their advantages such as high power density, fast charging-discharging rate and long lifespan [1,2]. According to the energy storage mechanism, supercapacitors are usually classified into electrochemical double layer capacitors (EDLC) and pseudocapacitors [3]. Owing to the high surface area and good conductivity, carbon-based materials typically carbon nanotubes, carbon quantum dots, graphene and activated carbon act as electrodes for EDLC [4]. The performance of asymmetric and hybrid supercapacitors is deeply affected by the specific capacitance of the negative electrodes. Therefore, there is an urgent need to concentrate more attention on the study of the negative electrode materials and explore new approaches to improve their specific capacitance to match with that of the corresponding positive electrodes.

Among carbon electrodes, graphene-based materials were extensively applied as the negative electrodes for asymmetric and hybrid supercapacitors due to their large working potential window and stability [1,2]. Graphene possesses promising potential for supercapacitor application, owing to its high theoretical specific capacitance (~550 F g^{-1} for a single-layer-graphene) [2,4]. Moreover, graphene exhibits excellent conductivity, favorable mechanical properties, chemical stability and large surface area, which are all beneficial for electrodes in supercapacitors. Although the literature on graphene-based electrode materials for supercapacitors is rich, the specific capacitance of pure graphene-based materials is far below the theoretical specific capacitance. The reduced specific capacitance recorded experimentally was attributed to the agglomeration of graphene layers because of the intense π-π interactions, which further decreases the active surface area to contact with the electrolyte. To improve the performance of graphene-based electrodes, surface functionalization represents a worth to investigate strategy. Among the different approaches to overcome graphene sheets' aggregation and improve their electrochemical performance, incorporation of conjugated molecules with suitable functional groups [5], transition metal oxides/hydroxides [6,7] and layered double hydroxides [7,8] have been widely investigated. The modern trend in the design of supercapacitors is directed towards the utilization of surface modification approaches such as π-π stacking on graphene structure, which conserves the π-conjugated structure and electrical conductivity of graphene system [9]. Nevertheless, non-covalent functionalization of graphene-based compounds with hydrophobic/aromatic molecules [10–13] lacks robustness during multiple charge-discharge processes. The covalent functionalization of reduced graphene oxide (rGO) is more advantageous than non-covalent approaches due to enhanced chemical/electrochemical stability of attached functional groups [9]. Several approaches for covalent grafting of functional groups onto rGO for supercapacitor application such as amide-

coupling [14–16], attachment of conducting polymers [17,18], diazonium functionalization [19–21], heteroatom doping [22,23] and azide cycloaddition [24] have recently been described. Among the various methods for covalent functionalization, the cycloaddition of benzyne can be considered as the most promising due to the conservation of intrinsic properties of graphene [25–28] and are still underdeveloped in the energy storage field.

Herein, we demonstrate a facile approach for the covalent grafting of fluorophenylene moieties *via* cycloaddition of 1-fluorobenzyne-2,3 intermediate onto rGO surface. The optimization of the reaction was carried out by varying the ratio between mesityl-2-fluoro-1-phenyboronic acid-6-iodonium triflate (MPB-OTf) as an aryne source and rGO［1/0.5 (f1-rGO), 1/0.83 (f2-rGO), 1/1 (f3-rGO)］. Among all obtained composites, f2-rGO exhibited the largest specific capacitance of 297 F g^{-1} at a current density of 1 A g^{-1}, which is larger than that attained by pristine rGO (170 F g^{-1} at 1 A g^{-1}) under otherwise identical conditions. Moreover, f2-rGO electrode was applied to construct a symmetric supercapacitor, which achieved a high energy density of 6.7 Wh kg^{-1} at a power density of 685.8 W kg^{-1} and successfully powered a home-designed windmill device for 3 s. To the best of our knowledge, this study represents the first report on rGO functionalization through benzyne cycloaddition reaction for supercapacitor application, opening more opportunities in the field of energy storage devices.

2. Experimental section

2.1. Materials

Reduced graphene oxide (rGO) was purchased from Graphitene Ltd (UK). 2-fluoro-6-iodophenylboronic acid (≥ 95%), acetic acid ((≥ 99.5%), mesitylene (≥ 97%), triflic acid (≥ 98%), methylene chloride (≥ 99%), potassium hydroxide (KOH), trifluoromethanesulfonic acid, N-methyl-2-pyrrolidone (NMP), polyvinylidene difluoride (PVDF), and ethanol (puriss p.a., absolute, ≥ 99.8%) were purchased from Sigma-Aldrich and used without further purification. Carbon paper (CP) was purchased from Maipengchen Electronic Technology Co., Ltd. (China). Nickel foam (NF) was obtained from Jiayisheng Company (China).

2.2. Functionalization of reduced graphene oxide (rGO) with mesityl-2-fluoro-1-phenyboronic acid-6-iodonium triflate (MPB-OTf)

Reduced graphene oxide (rGO) was added to a solution of MPB-OTf in methylene chloride/water (9/1 v/v) using different rGO/MPB-OTf (w/w) ratios: 1/0.5 (f1-rGO), 1/0.83 (f2-rGO), 1/1 (f3-rGO). The reaction mixture was sonicated for 3 h and then kept at room temperature overnight under stirring. The prepared material was separated by centrifugation,

washed with methylene chloride (3×), ethanol (3×), acetone (3×), and dried at T=60 °C for 24 hours.

2.3. Fabrication of a symmetric supercapacitor

To fabricate a symmetric supercapacitor device, f2-rGO was pasted on nickel foam (NF) with polyvinylidene difluoride (PVDF) in a mass ratio of 9:1. Using two as-prepared f2-rGO electrodes, a symmetric supercapacitor device was assembled with the separator consisting of a filter paper soaked into KOH (2 M) solution for 30 min.

The energy density (E, mWh kg^{-1}) and power density (P, mW kg^{-1}) of the symmetric supercapacitor cell can be determined from the specific capacitance using respectively equations (1) and (2):

$$E = \frac{0.5C \times \Delta V}{3600} \quad (1)$$

$$P = \frac{E \times 3600}{\Delta t} \quad (2)$$

where C (F g^{-1}) is the specific capacitance, ΔV (V) is the potential window of discharge, Δt (s) is the discharge time.

3. Results and discussion

3.1. Synthesis and characterization of functionalized reduced graphene oxide (f-rGO) samples

The reaction between reduced graphene oxide (rGO) and mesityl-2-fluoro-1-phenyboronic acid-6-iodonium triflate (MPB-OTf) was carried out in a mixture of dichloromethane/water. As has been described previously, the pseudocyclic mesityliodoxoborole triflate is able to interact with water to form extremely reactive aryne intermediate, upon elimination of mesityliodide and boric acid [29]. The high reactivity of MPB-OTf allows to conduct the process under mild conditions (room temperature) in comparison with methods reported earlier [25,26]. In order to estimate the influence of functionalization degree (the amount of attached functional groups), we prepared 3 batches of functionalized rGO using different MPB-OTf /rGO ratios of 1/0.5 (f1-rGO), 1/0.83 (f2-rGO), 1/1 (f3-rGO) (**Figure 1**).

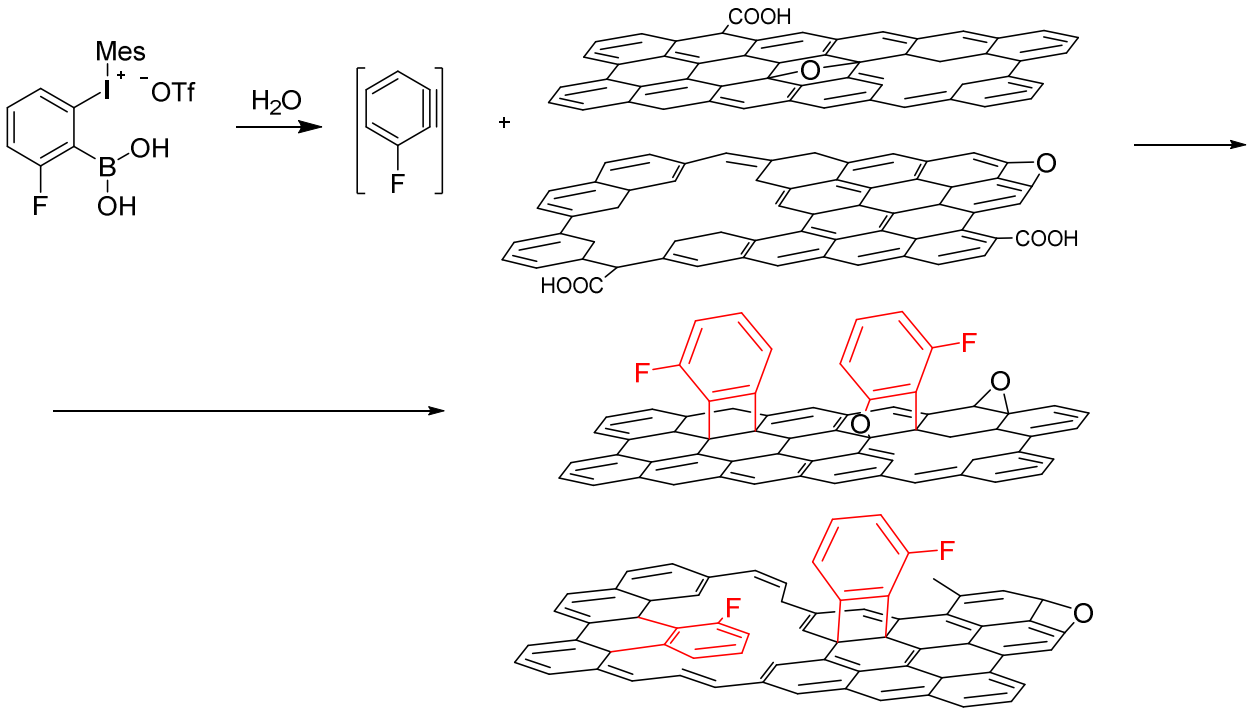

Figure 1. Schematic representation of aryne cycloaddition functionalization of rGO with MPB-OTf.

The functionalized rGO sheets were characterized using a number of spectroscopic techniques. The FTIR spectra of rGO, f1-rGO, f2-rGO, and f3-rGO are depicted in **Figure S1**. The FTIR spectrum of the pristine rGO revealed several characteristic vibration bands due to C=O (1730 cm^{-1}), C-O-C, C-OH (broad peak near 1300-1100 cm^{-1}), and C=C (1570 cm^{-1}) [30]. After functionalization with MPB-OTf, the presence of fluorophenylene moieties is difficult to discern; the stretching of the C-F bond at 1000-1150 cm^{-1} overlapped with aromatic C-H and C-O-C vibrations near 1000-1100 cm^{-1} [31]. Lee et al.[19] suggested a new approach for FTIR characterization of low functionalized surfaces. The aromatic C=C and C–C stretching band positions can be shifted by the conjugated system. Highly conjugated systems can cause a shift to higher wavenumber position for the aromatic C=C bond and lower wavenumber position for the aromatic C–C bond. The C–C stretching band position differences decrease from 336 nm to 346 nm respectively for f1-rGO and f3-rGO, supporting the presence of higher number of fluorophenylene moieties on rGO surface.

The XPS survey spectrum of pristine rGO (**Figure 2a**) exhibits characteristic peaks at 284.5 eV (C_{1s}) and 531.5 eV (O_{1s}). The calculated C/O ratio, which is a good indication of the reduction degree of rGO, was determined to be 8 for pristine rGO, suggesting high reduction degree [32]. After functionalization with MPB-OTf, an additional peak due to F_{1s} at around 686.5 eV was observed in the XPS survey spectrum (**Figure 2b** and **Figure S2**). A comparable

C/O ratio was obtained for the functionalized samples, testifying that cycloaddition of fluorobenzyne did not alter the content of oxidized carbon.

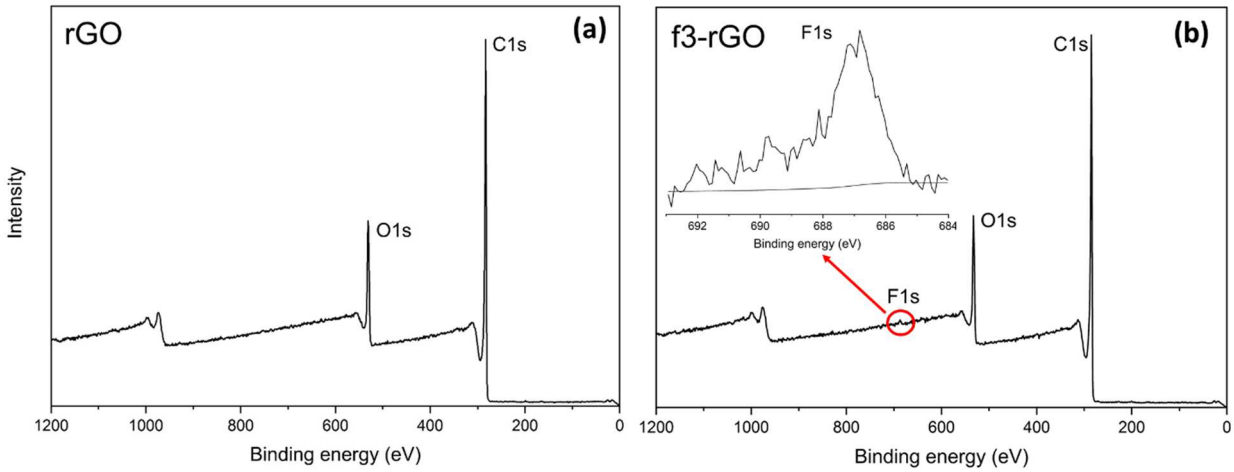

Figure 2. XPS survey spectra of (**a**) pristine rGO, and (**b**) f3-rGO. The inset is a zoom on the F_{1s} region.

The deconvolution of the C_{1s} region **(Figure S3)** of pristine rGO and functionalized f-rGO allows to identify Csp^2 (284.5 eV), C-O (286.1 eV), O-C=O (288.4 eV) and π-π* satellite (290.4 eV) [33]. For the functionalized f-rGO samples, C_{Ar}-F bond is difficult to recognize due to overlapping with O-C=O bond (288.4 eV) [25,34]. The peak at 290.4 eV assigned to π-π* (satellite) increases (**Table S1**), indicating the successful grafting of the fluorobenzene organic group on the surface [35].

The core level XPS spectrum of the O_{1s} in **Figure S4** can be curve-fitted with three bands ascribed to C=O (531.3 eV), C-OH (533.3 eV) and chemisorbed oxygen/H_2O (543.8 eV). The relative increase of the intensity of the C-O bond and simultaneous decrease of O-C=O bond after functionalization revealed the complex character of the modification process **(Figures S3, S4,** and **Table 1, Table S1)**. Thus, the generation of benzyne led to the addition of fluorophenylene moieties to the C=C bonds in the graphene structure and, also, the reaction with oxidized carbon involving oxygen atom [36].

After rGO functionalization with MPB-OTf, a peak at 686.8 eV (F_{1s}) was observed due to the covalent attachment of fluorobenzene moieties onto the rGO surface [30,34] **(Figures S2, S5)**. The high-resolution of the F_{1s} band **(Figure S5)** can be fitted with two peaks at 686.8 and 688.4 eV ascribed to C_{Ar}-F bond from grafted fluorophenylene functional group. The appearance of two peaks are most likely due to the complex character of interaction between aryne and rGO surface. Due to structural defects and presence of a wide range of O-containing functional groups on rGO surface, the reaction with aryne could potentially lead to fluorophenylene moieties in

different chemical environments (**Figure 1**). Taking into account that the position of C_{Ar}-F related peak is extremely sensitive to chemical substituents (684.5 - 688 eV) [37–39]), the 688.4 eV peak can be associated with different chemical environments.

The atomic percentages of C, O and F atoms for pristine rGO and f-rGO samples are summarized in **Table 1**; the bond contribution for each atom is displayed in **Table S1**. As we could see, by increasing the amount of MPB-OTf, the atomic concentration of F from attached fluorophenylene moieties increases slightly.

Table 1. Atomic percentages of different elements in pristine rGO, f1-rGO, f2-rGO and f3-rGO.

	C_{1s} (%)	O_{1s} (%)	F_{1s} (%)
rGO	86.60	13.40	-
f1-rGO	88.58	11.26	0.15
f2-rGO	88.18	11.62	0.16
f3-rGO	87.74	12.00	0.26

The optical properties of rGO before and after functionalization were assessed using UV–vis spectrophotometry. The UV-vis absorption spectrum of rGO exhibited characteristic absorbance of reduced graphene (black curve) with a maximum at around 269 nm (**Figure S6**) related to the electronic conjugation in graphene sheets [32]. The surface modification with fluorophenylene moieties did not lead to sufficient changes in the absorbance profile, indicating the conservation of the electronic conjugation in the graphene skeleton.

Raman spectroscopy is a powerful tool to study graphene-based materials. The Raman spectra of the samples revealed the presence of characteristic peaks of graphene-related materials: D (1360 cm^{-1}), G (1584 cm^{-1}), 2D (2690 cm^{-1}), D+G (2944 cm^{-1}) and 2D' (3180 cm^{-1}) bands (**Figure 3**) [40]. The vibration of the C-F bond from the modified samples was observed at 923-1023 cm^{-1} [31] only in case of f3-rGO sample, where the concentration of MPB-OTf was the highest. The appearance of a band at 515 cm^{-1} in f3-rGO is associated with C-H in-plane and out-of-plane bending modes of organic functional groups [26,31,41].

The analysis of the ratio between I_D/I_G peak intensities did not reveal significant changes of defect concentration in the modified rGO (rGO: 0.685; f1-rGO: 0.669; f2-rGO: 0.732; f3-rGO: 0.641). The low defect concentration was reported earlier in case of functionalization of pure graphene with benzyne moieties [26,28,42]. Maio et al. [37] suggested a new approach for the characterization of low functionalized surfaces. The spectra were fitted by means of Gauss curves (**Figure 4**) and the analysis was focused on the evolution of two additional contributions, named Ω mode, centered at 1180 cm^{-1} and assigned to C-O-C bond, and Φ mode, located at

1525 cm^{-1} and ascribed to C=C bond in phenyl ring. While the I_D/I_G is almost unaltered for the functionalized samples, the intensity of the D mode is slightly increased due to appearance of additional fluorophenylene moieties on the surface and at the same time the intensity of the G mode peak also increases, suggesting introduction of new graphenic sp^2 domains from attached fluorophenylene moieties. On the other hand, the Ω mode of f-rGO samples decreases probably due to involvement of C-O-C bond instead of epoxy band in fluorophenylene moieties grafted on the surface [36].

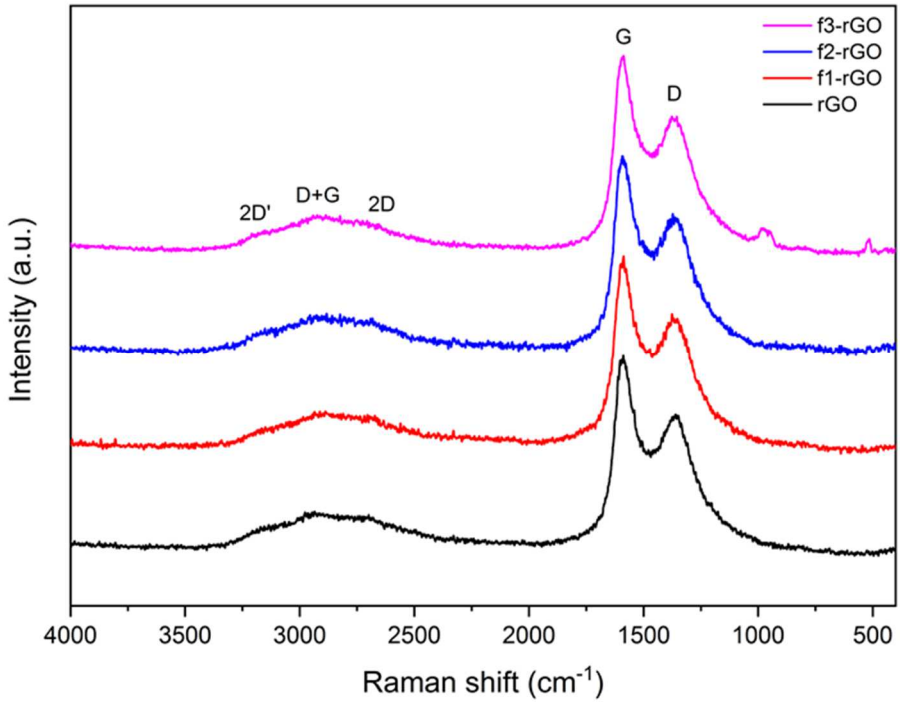

Figure 3. Raman spectra of rGO before and after functionalization with MPB -OTf.

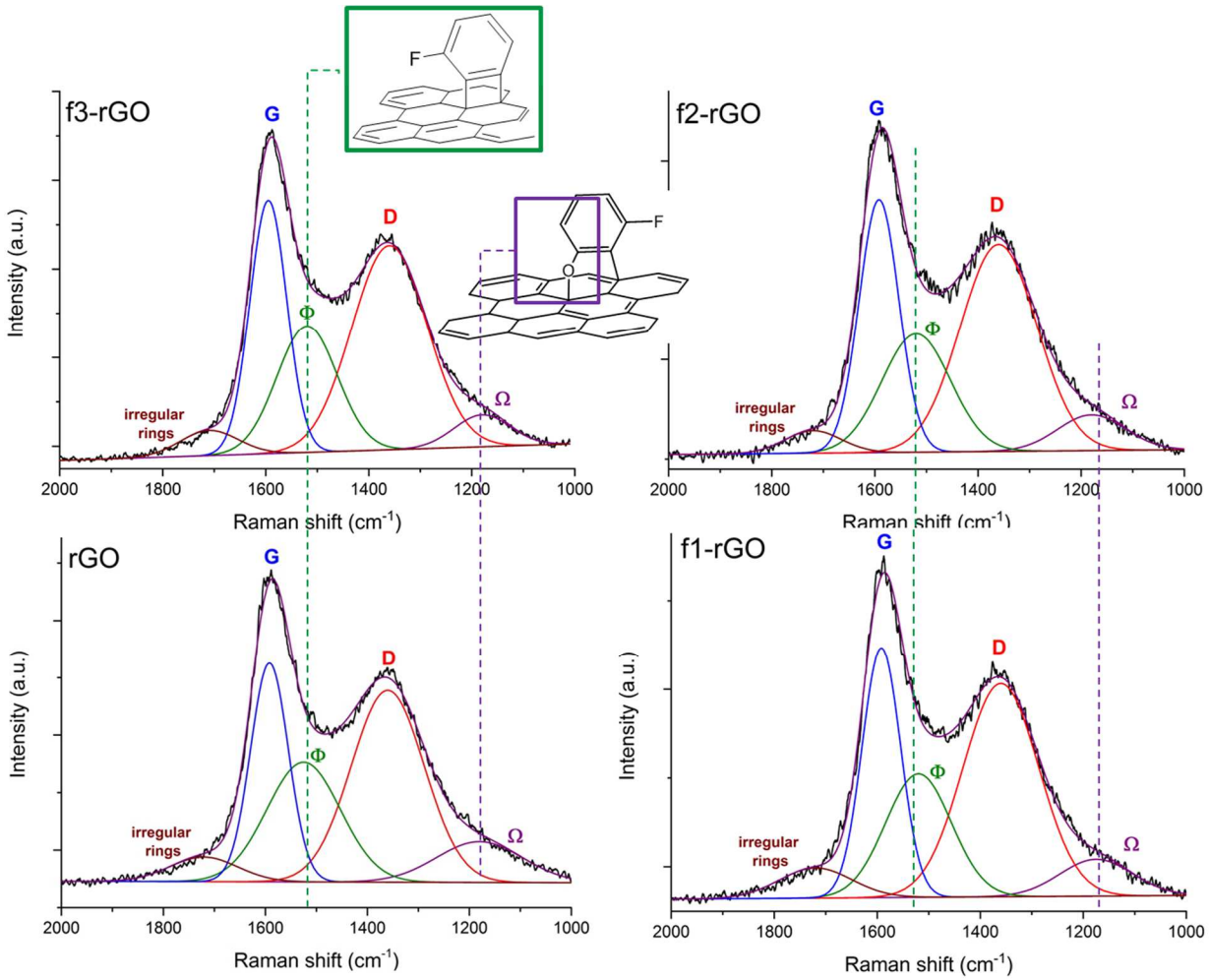

Figure 4. Micro-Raman plots of rGO and f-rGO samples fitted by means of Gauss peaks to examine the contribution and evolution of D and G modes together with those of the bands associated with C-O-C bonds (Ω, centered at 1160 cm^{-1}), phenyl rings (Φ, centered at 1525 cm^{-1}) and irregular rings (located at 1700–1750 cm^{-1}).

The powder X-ray diffraction (XRD) patterns are depicted in **Figure S7.** XRD pattern of pristine rGO exhibited a weak intensity peak at 24.6° (002 plane) typical for rGO. After reaction with fluorobenzyne, analysis of XRD pattern of f-rGO did not reveal significant changes.

Transmission electron microscopy (TEM) was used for the determination of the average lateral distance of rGO and f-rGO samples, which could affect the electrolyte mobility in the structure during the measurement and energy storage application (**Figures 5** and **Figures S8, S9**) [43]. The average lateral distance of rGO is 0.386±0.017 nm that agrees well with the commonly observed interlayer distance of rGO (0.38 nm) [19]. All functionalized f-rGO samples display larger lateral distance than rGO (f1-rGO: 0.462±0.018 and f2-rGO: 0.467±0.036 nm), which can be explained by the presence of fluorophenylene moieties on the surface of the graphene sheets.

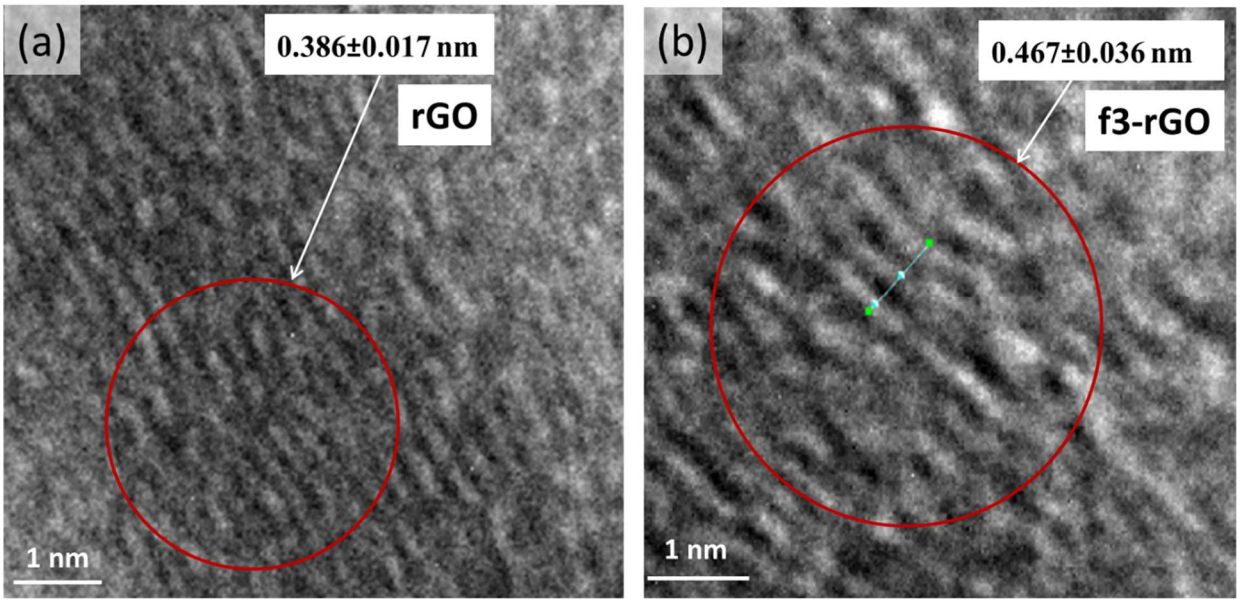

Figure 5. Transmission electron microscopy (TEM) images of (a) rGO and (b) f3-rGO.

3.2. Electrochemical properties

The electrochemical performance of the as-obtained f-rGO samples was explored in a 3-electrode cell containing 2 M KOH electrolyte (**Figure 6**). **Figure 6a** depicts the cyclic voltammetry (CV) curves of the samples measured at a scan rate of 100 mV s^{-1}, which shows a similar rectangular shape with a slight deformation in the potential window from -0.9 to +0.3 V. Among all the composites, f2-rGO manifests the largest CV area and enhanced current density, demonstrating the largest specific capacitance. In **Figure 6b**, we can see that the CV shapes of f2-rGO composite are retained as the scan rate increases, indicating good capacitive performance.

Galvanostatic charge-discharge (GCD) curves of all samples were recorded and displayed in **Figure 6c**. It is obvious that the f2-rGO sample exhibits the largest specific capacitance of 297 F g^{-1} at a current density of 1 A g^{-1}. According to **Figure 6d** and equation **S1**, the specific capacitance values of f2-rGO were calculated as 254, 243, 234 and 230 F g^{-1} at current densities of 2, 3, 4 and 5 A g^{-1}, respectively, suggesting a favorable rate performance (**Figure 6e** and **Table 2**). Even though f3-rGO contains the highest fluorine content, it displays a relatively lower specific capacitance of 244, 208, 198, 192 and 190 F g^{-1} at 1, 2, 3, 4 and 5 A g^{-1}, respectively. The specific capacitance value of f2-rGO is higher than that reported in the literature for rGO-based materials (**Table 3**), revealing the importance of rGO functionalization with MPB-OTf. At the same time, all the samples display high coulombic efficiencies (**Table S2**), indicating their potential application for supercapacitor electrodes.

The electrochemical performance of the functionalized rGO can be explained by the balance between the degree of functionalization and interlayer distance between flakes. Previously, Song

et al. [15] reported the covalent functionalization of rGO with p-phenylenediamine (PPD) monomers *via* nucleophilic substitution between amino groups and epoxy groups of rGO for enlargement of graphene interlayer spacing. The best electrochemical properties were achieved by the covalent attachment of PPD on rGO surface, producing material with the largest specific capacitance of 339 F g^{-1} at 100 mV s^{-1} and graphene interlayer spacing of 1.41 nm. Lee at al. [19] designed molecularly gap-controlled reduced graphene oxides (rGOs) *via* diazotization of three different phenyl, biphenyl (BD), and *para*-terphenyl bis-diazonium salts. The rGO−BD2 (0.7 nm gap) achieved the highest capacitance of 250 F g^{-1} at 100 mA g^{-1} in 6 M KOH and 165.98 F g^{-1} at 100 mA g^{-1} in 1 M $TEABF_4$. Banda et al. [44] described pillared graphene materials, designed by cross-linking graphene sheets with a bifunctional pillar molecule and the resulting interconnected porous network achieved gravimetric capacitance values two-times greater than that of rGO (200 $F \cdot g^{-1}$ *vs.* 107 $F \cdot g^{-1}$) and volumetric capacitances that are nearly four-times larger (210 $F \cdot cm^{-3}$ *vs.* 54 $F \cdot cm^{-3}$).

The capacitance of f-rGO is determined by several factors: the conservation of electronic structure of rGO and the increase of the distance between flakes, leading to better accessibility and mobility of the electrolyte ions to modified graphene sheets, as reported previously [19,45,46]. The aryne cycloaddition led to the attachment of relatively low number of functional groups, which did not affect dramatically the conductive properties of rGO. At the same time, the presence of fluorophenylene moieties allowed to increase the interlayer distance and provide better transport properties for electrolyte ions. The combination of the two factors offers an enhanced capacitance in comparison with more traditional modification methods utilizing diazonium chemistry [47–49].

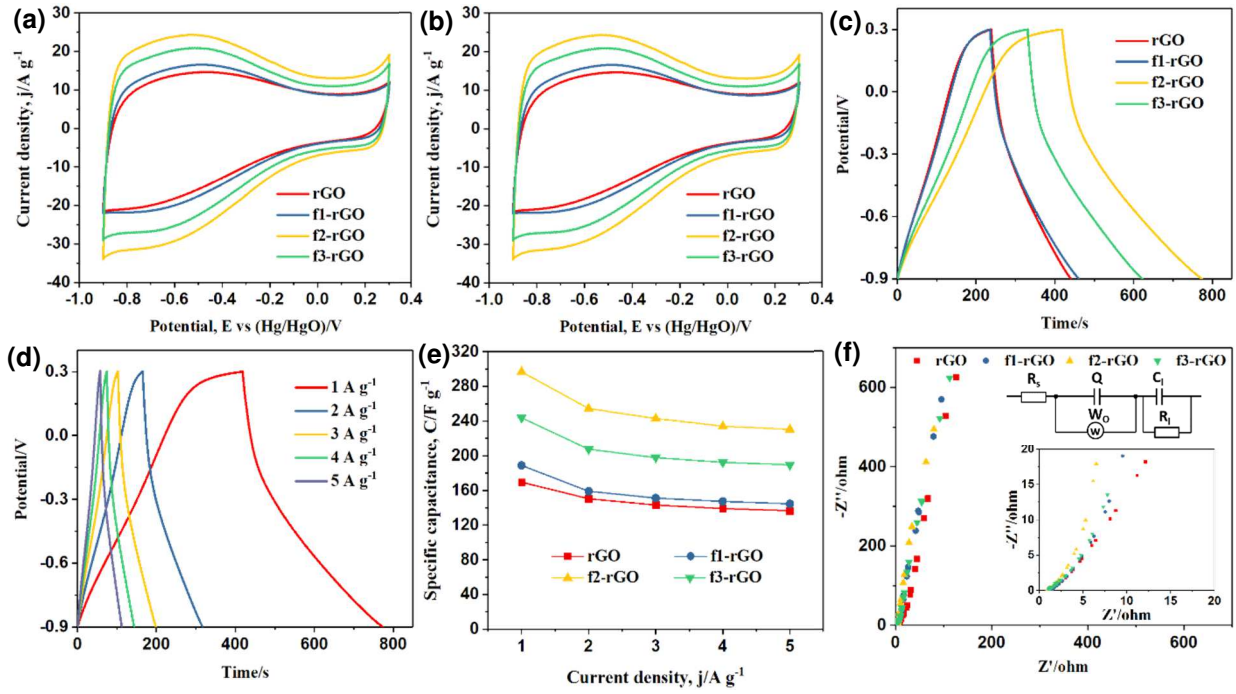

Figure 6: The electrochemical performance of the electrodes measured in a classical three-electrode configuration cell containing 2 M KOH aqueous solution. (**a**) CV curves measured at a scan rate of 100 mV s^{-1}. (**b**) CV curves of f2-rGO recorded at different scan rates. (**c**) GCD plots of the electrodes acquired at a current density of 1 A g^{-1}. (**d**) GCD profiles of f2-rGO at various current densities. (**e**) Specific capacitance at different current densities. (**f**) Electrochemical impedance spectra recorded at open circuit potential in the frequency range from 0.01 Hz to 100 kHz, the inset in the top-right of (**f**) is the corresponding equivalent circuit.

Table 2. The specific capacitance (C/F g^{-1}) of rGO and f-rGO electrode materials.

Current density, j/A g^{-1} / **Samples**	**1**	**2**	**3**	**4**	**5**
rGO	169.5	150.4	143.2	139.1	136.7
f1-rGO	188.9	159.0	151.2	147.3	144.5
f2-rGO	296.9	254.4	242.9	234.1	230.4
f3-rGO	243.7	207.6	197.8	192.3	189.5

At the same time, EIS of the samples was conducted to further analyze the ion diffusion in low-frequency region and charge transfer resistance in high-to-medium frequency region. As illustrated in **Figure 6f**, a straight line almost parallel to the Y-axis was observed, indicating fast ion diffusion in the electrode material. There was no obvious semicircle in the low-frequency

region because of the fast charge transfer, corresponding to the electrochemical impedance equivalent circuit displayed in the inset of **Figure 6f** (R_s, Q, W_o, C_l and R_l are respectively the internal resistance, pseudocapacitance, Warburg element, limit capacitance and limit resistance). The intrinsic resistance of the samples was further determined. For pure rGO, the value is 1.13 ohm cm^{-2}, and 1.36, 0.93 and 1.34 ohm cm^{-2} for f1-rGO, f2-rGO and f3-rGO, respectively. All the results evidence the favorable conductivity of the as-prepared samples.

Table 3. Comparison of electrochemical performance of graphene-based supercapacitors.

Electrode material	**Electrolyte**	**Modification method**	**Specific capacitance, C/F g^{-1}**	**Ref.**
Laser reduced graphene	0.5 M Na_2SO_4	Laser irradiation reduction	141 at 1.04 A g^{-1}	[50]
rGOs	6 M KOH	Electron beam irradiation reduction	206.8 at 0.2 A g^{-1}	[51]
PPD/rGO	1 M H_2SO_4	Nucleophilic substitution	339 at 100 mV s^{-1}	[15]
rGO–BD2	6 M KOH and 1 M $TEABF_4$ /propylene carbonate (PC)	Diazonium chemistry	250 at 100 mA g^{-1} (6 M KOH) 165.98 at 100 mA g^{-1} (1 M $TEABF_4$)	[19]
N-RGO	6 M KOH	ice-templating method	217 at 5 mV s^{-1}	[52]
Crumpled nitrogen-doped graphene nanosheets (GO)	1.0 M [Bu_4 N]BF_4 acetonitrile	Hummer's method; polymerization	245.9 at 1 A g^{-1}	[53]
Cl-rGO	1 M H_2SO_4	Heteroatom doping	178.4 at 1 A g^{-1}	[54]
B-G12 (GO)	6 M KOH	Heteroatom doping	34.6 at 0.1 A g^{-1}	[55]
f-RGOF	1 M H_2SO_4	heat pressing method with crumpled topography (Fluffy layered structure)	238.4 at 0.5 A g^{-1}	[56]
Pillared rGO	1 M solution of	separating with a pillar molecule	190 at 0.01 V s^{-1}	[44]

	$TAABF_4$ in acetonitrile			
f2-rGO	2 M KOH	Benzyne cycloaddition	297 at 1 A g^{-1}	This work

3.3. Fabrication of a symmetric supercapacitor

Furthermore, a symmetric supercapacitor device was assembled using two f2-rGO electrodes, according to the schematic diagram presented in **Figure 7a**. The electrochemical performance was assessed in a 2-electrode system. CV curves with different cell potential windows at 100 mV s^{-1} were measured to explore the suitable working conditions. From **Figure 7b**, we can see that the symmetric supercapacitor device could operate from 0 to 1.4 V. Owing to the polarization phenomenon occurring at potentials larger than 1.3 V, 0-1.3 V was selected as the operating cell potential window to reduce the damage to the electrodes and ensure stable operation of the device.

Figure 7c depicts the CV plots obtained between 0 and 1.3 V at various scan rates, which exhibit a typical capacitive-like behavior of a symmetric supercapacitor device with obvious deviation from ideal capacitive characteristics. According to equation **S1** and GCD curves displayed in **Figure 7d**, the specific capacitance values of the device were calculated as 24, 28, 27, 25, 25 and 23 F g^{-1} at respectively 1, 2, 3, 4, 6 and 8 A g^{-1} (**Figure 7e**). Accordingly, the corresponding energy and power densities were determined by using equations (1) and (2) and described in the Ragone plot in **Figure 7f**, achieving the largest energy density of 6.7 Wh kg^{-1} at a power density of 685.8 W kg^{-1}, which is higher than that achieved by aRGO20//aRGO20 (4.7 and 4 Wh kg^{-1} at 402 and 1989 W kg^{-1}) [57], ACN−700//ACN−700 (6.2 Wh kg^{-1} at 300 W kg^{-1}) [58] symmetric supercapacitor devices, symmetric SBGO-(1: 2) cell (5.1 Wh kg^{-1} at 496 W kg^{-1}) [59], symmetric SCBAGO cell (5.3 Wh kg^{-1} at 502 W kg^{-1}) [60], symmetric SGO-(1:2) cell (4.4 Wh kg^{-1} at 495 W kg^{-1}) [61], and AOGO-(1:2) symmetric cell (5.5 Wh kg^{-1} at 495 W kg^{-1}) [62].

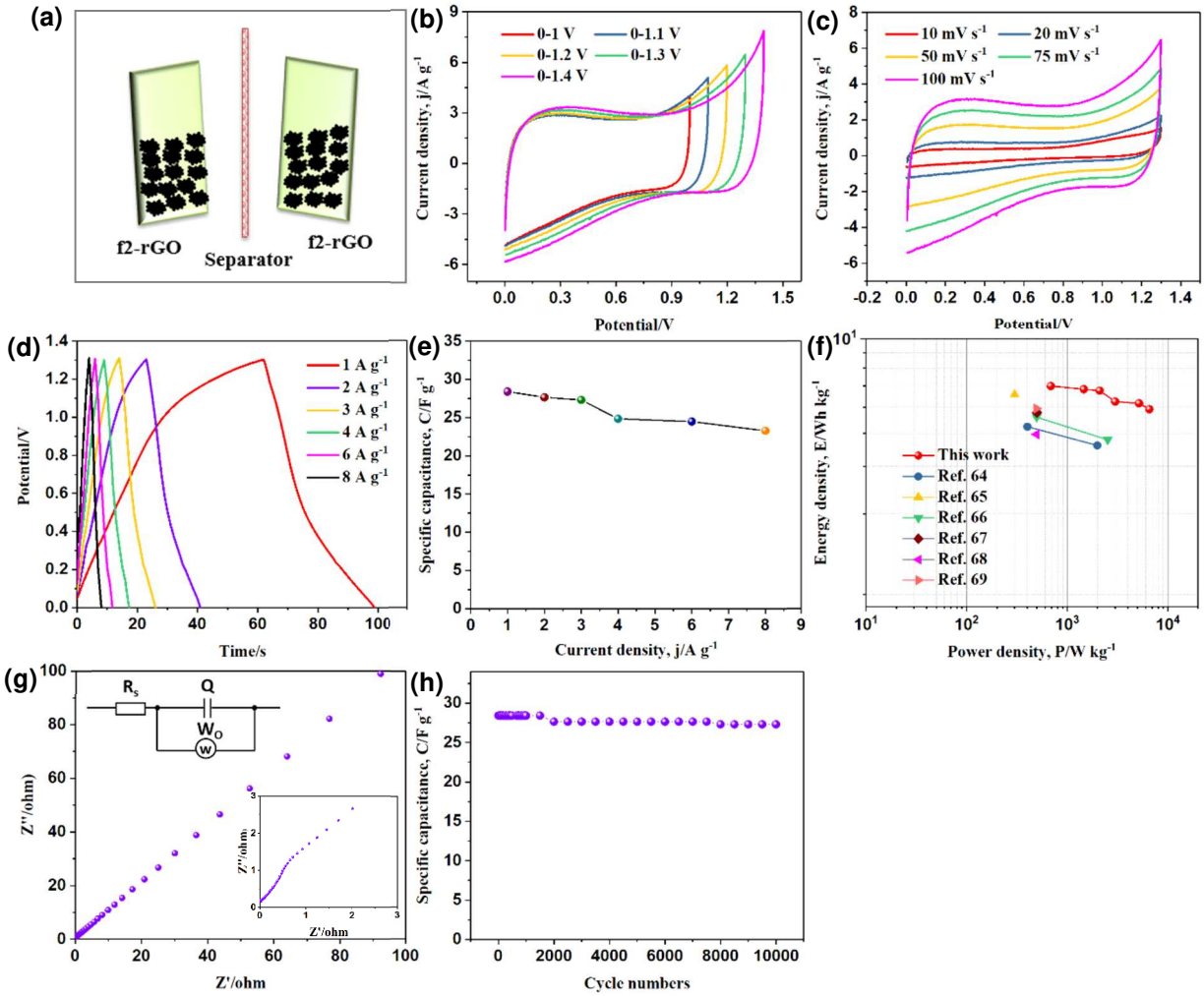

Figure 7: (**a**) Schematic of the packed symmetric supercapacitor device. CV plots measured at 100 mV s^{-1} at (**b**) different potential windows, and (**c**) various scan rates between 0 and 1.3 V. (**d**) GCD curves recorded at various current densities. (**e**) Specific capacitance at different current densities. (**f**) Ragone plot. (**g**) EIS curve acquired in the frequency range of 0.01 Hz and 100 kHz, the inset in the top-left of (g) is the corresponding equivalent circuit. (**h**) Cycling performance at 1 A g^{-1}.

EIS was further measured to analyze the ion diffusion in low-frequency region and charge transfer resistance in high-to-medium frequency region of the symmetric supercapacitor device. Similar to the single electrode, there exists no obvious semicircle in the low-frequency region of **Figure 7g** because of the fast charge transfer, indicating the excellent conductivity of the electrode, consistent with the equivalent circuit. The intrinsic resistance of the device was 0.06 ohm cm^{-2}. Additionally, the stability was tested for 10.000 charging-discharging cycles at 1 A g^{-1}. The device maintained about 96% of the initial capacitance value after 10,000 cycles, suggesting a good cycling stability.

To further explore the practical applicability of the device, two as-fabricated symmetric supercapacitor (SC) devices were connected in series to provide power for a home-designed windmill device including an engine (1.5-9 V) and a windmill, as shown in **Figure 8a**, and the cell voltage window of the two devices can reach up to 2.6 V (**Figure 8b**). From **Figure 8c**, we can observe that the two as-fabricated symmetric supercapacitor devices can successfully supply energy for the home-designed windmill device, lasting for 3 s.

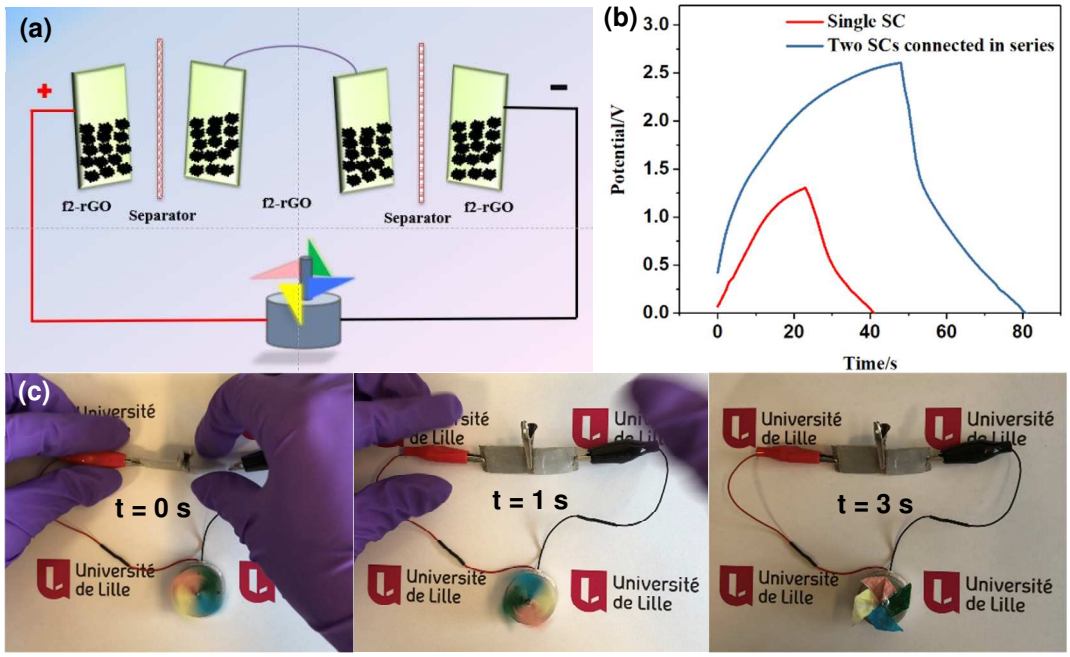

Figure 8: (**a**) Schematic of two symmetric supercapacitor cells operating a homemade windmill device. (**b**) GCD curves of a single supercapacitor (SC) and two supercapacitors in series. (**c**) Photographs of the home-designed windmill device operation.

4. Conclusion

In summary, reduced graphene oxide (rGO) was chemically functionalized by fluorophenylene group using aryne cycloaddition reaction under mild conditions. The successful covalent grafting of fluorophenylene moieties on the rGO surface was supported by several surface analysis techniques. XPS analysis confirmed the covalent grafting *via* the appearance of marker element -F from the fluorophenylene group. The XPS and Raman results suggest a successful, but low degree of surface functionalization. TEM analysis showed an increase of the interlayer distance from 0.38 to 0.46 nm upon functionalization due to the presence of fluorophenylene moieties. The electrochemical properties of the functionalized rGO materials were assessed by CV, GCD and EIS measurements. The largest specific capacitance value was recorded for the f2-rGO sample reaching 297 F g^{-1} at a current density of 1 A g^{-1}, which is larger than that of pristine rGO (170 F g^{-1} at 1 A g^{-1}). The enhancement of f-rGO capacitance could be

ascribed to the low degree of functionalization conserving the conductivity and the increase of interlayer distance between agglomerated graphene layers providing enhanced transport property for electrolyte ions in the material. Therefore, in our study is introduced a new functionalization method of graphene surface by benzyne cycloaddition reaction from iodonium compounds for improving the specific capacitance of electrode materials for energy storage devices.

Acknowledgement.

The research was supported by Russian Science Foundation (RSF № 17-73-20066). PSP and SVE thanks M. Syrtanov (TPU) for the XRD measurements. Financial support from the Centre National de la Recherche Scientifique (CNRS), the University of Lille and the Hauts-de-France region is acknowledged.

References

[1] X. Li, L. Zhi, Graphene hybridization for energy storage applications, Chem. Soc. Rev. 47 (2018) 3189–3216. https://doi.org/10.1039/C7CS00871F.

[2] K. Chen, S. Song, F. Liu, D. Xue, Structural design of graphene for use in electrochemical energy storage devices, Chem. Soc. Rev. 44 (2015) 6230–6257. https://doi.org/10.1039/C5CS00147A.

[3] A. Noori, M.F. El-Kady, M.S. Rahmanifar, R.B. Kaner, M.F. Mousavi, Towards establishing standard performance metrics for batteries, supercapacitors and beyond, Chem. Soc. Rev. 48 (2019) 1272–1341. https://doi.org/10.1039/c8cs00581h.

[4] L. Liu, Z. Niu, J. Chen, Unconventional supercapacitors from nanocarbon-based electrode materials to device configurations, Chem. Soc. Rev. 45 (2016) 4340–4363. https://doi.org/10.1039/C6CS00041J.

[5] R. Naz, M. Imtiaz, Q. Liu, L. Yao, W. Abbas, T. Li, I. Zada, Y. Yuan, W. Chen, J. Gu, Highly defective 1T-MoS2 nanosheets on 3D reduced graphene oxide networks for supercapacitors, Carbon 152 (2019) 697–703. https://doi.org/10.1016/j.carbon.2019.06.009.

[6] Y. Wang, W. Lai, N. Wang, Z. Jiang, X. Wang, P. Zou, Z. Lin, H.J. Fan, F. Kang, C.-P. Wong, C. Yang, A reduced graphene oxide/mixed-valence manganese oxide composite electrode for tailorable and surface mountable supercapacitors with high capacitance and super-long life, Energy Environ. Sci. 10 (2017) 941–949. https://doi.org/10.1039/C6EE03773A.

[7] H. Ma, J. He, D.-B. Xiong, J. Wu, Q. Li, V. Dravid, Y. Zhao, Nickel Cobalt Hydroxide @Reduced Graphene Oxide Hybrid Nanolayers for High Performance Asymmetric

Supercapacitors with Remarkable Cycling Stability, ACS Appl. Mater. Interfaces 8 (2016) 1992–2000. https://doi.org/10.1021/acsami.5b10280.

[8] M. Li, R. Jijie, A. Barras, P. Roussel, S. Szunerits, R. Boukherroub, NiFe layered double hydroxide electrodeposited on Ni foam coated with reduced graphene oxide for high-performance supercapacitors, Electrochim. Acta 302 (2019) 1–9. https://doi.org/10.1016/j.electacta.2019.01.187.

[9] V. Georgakilas, M. Otyepka, A.B. Bourlinos, V. Chandra, N. Kim, K.C. Kemp, P. Hobza, R. Zboril, K.S. Kim, Functionalization of Graphene: Covalent and Non-Covalent Approaches, Derivatives and Applications, Chem. Rev. 112 (2012) 6156–6214. https://doi.org/10.1021/cr3000412.

[10] B. Vedhanarayanan, B. Babu, M.M. Shaijumon, A. Ajayaghosh, Exfoliation of Reduced Graphene Oxide with Self-Assembled π-Gelators for Improved Electrochemical Performance, ACS Appl. Mater. Interfaces 9 (2017) 19417–19426. https://doi.org/10.1021/acsami.6b09418.

[11] L. Hou, C. Kong, Z. Hu, Y. Yang, H. Wu, Z. Li, X. Wang, P. Yan, X. Feng, Non-covalently self-assembled organic molecules graphene aerogels to enhance supercapacitive performance, Appl. Surf. Sci. 508 (2020) 145192. https://doi.org/10.1016/j.apsusc.2019.145192.

[12] C. Zhou, T. Gao, Q. Liu, Y. Wang, D. Xiao, Preparation of quinone modified graphene-based fiber electrodes and its application in flexible asymmetrical supercapacitor, Electrochim. Acta 336 (2020) 135628. https://doi.org/10.1016/j.electacta.2020.135628.

[13] S. Li, X. Wang, L. Hou, X. Zhang, Y. Zhou, Y. Yang, Z. Hu, Graphene hydrogels functionalized non-covalently by fused heteroaromatic molecule for asymmetric supercapacitor with ultra-long cycle life, Electrochim. Acta 317 (2019) 437–448. https://doi.org/10.1016/j.electacta.2019.06.022.

[14] P. Bandyopadhyay, T.T. Nguyen, N.H. Kim, J.H. Lee, Facile synthesis of 4,4′-diaminostilbene-2,2′-disulfonic-acid-grafted reduced graphene oxide and its application as a high-performance asymmetric supercapacitor, Chem. Eng. J. 333 (2018) 170–184. https://doi.org/10.1016/j.cej.2017.09.157.

[15] B. Song, J. Il Choi, Y. Zhu, Z. Geng, L. Zhang, Z. Lin, C. Tuan, K. Moon, C. Wong, Molecular Level Study of Graphene Networks Functionalized with Phenylenediamine Monomers for Supercapacitor Electrodes, Chem. Mater. 28 (2016) 9110–9121. https://doi.org/10.1021/acs.chemmater.6b04214.

[16] M. Jana, P. Khanra, N.C. Murmu, P. Samanta, J.H. Lee, T. Kuila, Covalent surface modification of chemically derived graphene and its application as supercapacitor

electrode material, Phys. Chem. Chem. Phys. 16 (2014) 7618. https://doi.org/10.1039/c3cp54510e.

[17] N.A. Kumar, H.-J. Choi, Y.R. Shin, D.W. Chang, L. Dai, J.-B. Baek, Polyaniline-Grafted Reduced Graphene Oxide for Efficient Electrochemical Supercapacitors, ACS Nano 6 (2012) 1715–1723. https://doi.org/10.1021/nn204688c.

[18] Z. Chen, W. Liao, X. Ni, Spherical polypyrrole nanoparticles growing on the reduced graphene oxide-coated carbon cloth for high performance and flexible all-solid-state supercapacitors, Chem. Eng. J. 327 (2017) 1198–1207. https://doi.org/10.1016/j.cej.2017.06.098.

[19] K. Lee, Y. Yoon, Y. Cho, S.M. Lee, Y. Shin, H. Lee, H. Lee, Tunable Sub-nanopores of Graphene Flake Interlayers with Conductive Molecular Linkers for Supercapacitors, ACS Nano 10 (2016) 6799–6807. https://doi.org/10.1021/acsnano.6b02415.

[20] K. Jo, M. Gu, B.-S. Kim, Ultrathin Supercapacitor Electrode Based on Reduced Graphene Oxide Nanosheets Assembled with Photo-Cross-Linkable Polymer: Conversion of Electrochemical Kinetics in Ultrathin Films, Chem. Mater. 27 (2015) 7982–7989. https://doi.org/10.1021/acs.chemmater.5b03296.

[21] H.A. Alinajafi, A.A. Ensafi, B. Rezaei, Reduced graphene oxide decorated with thionine, excellent nanocomposite material for a powerful electrochemical supercapacitor, Int. J. Hydrogen Energy 43 (2018) 19102–19110. https://doi.org/10.1016/j.ijhydene.2018.08.142.

[22] S.K. Singh, V.M. Dhavale, R. Boukherroub, S. Kurungot, S. Szunerits, N-doped porous reduced graphene oxide as an efficient electrode material for high performance flexible solid-state supercapacitor, Appl. Mater. Today 8 (2017) 141–149. https://doi.org/10.1016/j.apmt.2016.10.002.

[23] X. Fan, H. Xu, S. Zuo, Z. Liang, S. Yang, Y. Chen, Preparation and supercapacitive properties of phosphorus-doped reduced graphene oxide hydrogel, Electrochim. Acta 330 (2020) 135207. https://doi.org/10.1016/j.electacta.2019.135207.

[24] R. Teimuri-Mofrad, R. Hadi, H. Abbasi, Synthesis and characterization of ferrocene-functionalized reduced graphene oxide nanocomposite as a supercapacitor electrode material, J. Organomet. Chem. 880 (2019) 355–362. https://doi.org/10.1016/j.jorganchem.2018.11.033.

[25] X. Zhong, J. Jin, S. Li, Z. Niu, W. Hu, R. Li, J. Ma, Aryne cycloaddition: highly efficient chemical modification of graphene, Chem. Commun. 46 (2010) 7340–7342. https://doi.org/10.1039/C0CC02389B.

[26] I. V Magedov, L. V Frolova, M. Ovezmyradov, D. Bethke, E.A. Shaner, N.G. Kalugin,

Benzyne-functionalized graphene and graphite characterized by Raman spectroscopy and energy dispersive X-ray analysis, Carbon 54 (2013) 192–200. https://doi.org/10.1016/j.carbon.2012.11.025.

[27] M. Hammouri, S.K. Jha, I. Vasiliev, First-Principles Study of Graphene and Carbon Nanotubes Functionalized with Benzyne, J. Phys. Chem. C 119 (2015) 18719–18728. https://doi.org/10.1021/acs.jpcc.5b04065.

[28] M. V Sulleiro, S. Quiroga, D. Peña, D. Pérez, E. Guitián, A. Criado, M. Prato, Microwave-induced covalent functionalization of few-layer graphene with arynes under solvent-free conditions, Chem. Commun. 54 (2018) 2086–2089. https://doi.org/10.1039/C7CC08676H.

[29] A. Yoshimura, J.M. Fuchs, K.R. Middleton, A. V Maskaev, G.T. Rohde, A. Saito, P.S. Postnikov, M.S. Yusubov, V.N. Nemykin, V. V Zhdankin, Pseudocyclic Arylbenziodoxaboroles: Efficient Benzyne Precursors Triggered by Water at Room Temperature, Chem. – A Eur. J. 23 (2017) 16738–16742. https://doi.org/10.1002/chem.201704393.

[30] Y.J. Oh, J.J. Yoo, Y. Il Kim, J.K. Yoon, H.N. Yoon, J.-H. Kim, S. Bin Park, Oxygen functional groups and electrochemical capacitive behavior of incompletely reduced graphene oxides as a thin-film electrode of supercapacitor, Electrochim. Acta 116 (2014) 118–128. https://doi.org/10.1016/j.electacta.2013.11.040.

[31] J. Coates, Interpretation of Infrared Spectra, A Practical Approach, Encycl. Anal. Chem. (2006). https://doi.org/10.1002/9780470027318.a5606.

[32] Y. Chen, X. Zhang, D. Zhang, P. Yu, Y. Ma, High performance supercapacitors based on reduced graphene oxide in aqueous and ionic liquid electrolytes, Carbon 49 (2011) 573–580. https://doi.org/10.1016/j.carbon.2010.09.060.

[33] R.D. Rodriguez, G. V Murastov, A. Lipovka, M.I. Fatkullin, O. Nozdrina, S.K. Pavlov, P.S. Postnikov, M.M. Chehimi, J.-J. Chen, E. Sheremet, High-power laser-patterning graphene oxide: A new approach to making arbitrarily-shaped self-aligned electrodes, Carbon 151 (2019) 148–155. https://doi.org/10.1016/j.carbon.2019.05.049.

[34] W. Feng, P. Long, Y. Feng, Y. Li, Two-Dimensional Fluorinated Graphene: Synthesis, Structures, Properties and Applications, Adv. Sci. 3 (2016) 1500413. https://doi.org/10.1002/advs.201500413.

[35] R. Blume, D. Rosenthal, J.-P. Tessonnier, H. Li, A. Knop-Gericke, R. Schlögl, Characterizing Graphitic Carbon with X-ray Photoelectron Spectroscopy: A Step-by-Step Approach, ChemCatChem. 7 (2015) 2871–2881. https://doi.org/10.1002/cctc.201500344.

[36] S. Beltrán-Rodil, D. Peña, E. Guitián, Reaction of Benzyne with Styrene Oxide: Insertion

of Arynes into a C-O Bond of Epoxides, Synlett 2007 (2007) 1308–1310. https://doi.org/10.1055/s-2007-977460.

[37] A. Maio, R. Scaffaro, L. Lentini, A. Palumbo Piccionello, I. Pibiri, Perfluorocarbons–graphene oxide nanoplatforms as biocompatible oxygen reservoirs, Chem. Eng. J. 334 (2018) 54–65. https://doi.org/https://doi.org/10.1016/j.cej.2017.10.032.

[38] M. Weissmann, S. Baranton, C. Coutanceau, Modification of Carbon Substrates by Aryl and Alkynyl Iodonium Salt Reduction, Langmuir 26 (2010) 15002–15009. https://doi.org/10.1021/la1024313.

[39] S.M. Park, H. Yu, M.G. Park, S.Y. Han, S.W. Kang, H.M. Park, J.W. Kim, Quantitative analysis of an organic thin film by XPS, AFM and FT-IR, Surf. Interface Anal. 44 (2012) 156–161. https://doi.org/10.1002/sia.3786.

[40] R. Saito, M. Hofmann, G. Dresselhaus, A. Jorio, M.S. Dresselhaus, Raman spectroscopy of graphene and carbon nanotubes, Adv. Phys. 60 (2011) 413–550. https://doi.org/10.1080/00018732.2011.582251.

[41] F. Menaa, B. Menaa, O. Sharts, Development of carbon-fluorine spectroscopy for pharmaceutical and biomedical applications, Faraday Discuss. 149 (2011) 269–278. https://doi.org/10.1039/C005252C.

[42] A. Criado, M. Melchionna, S. Marchesan, M. Prato, The Covalent Functionalization of Graphene on Substrates, Angew. Chem. Int. Ed. 54 (2015) 10734–10750. https://doi.org/10.1002/anie.201501473.

[43] B. Pal, S. Yang, S. Ramesh, V. Thangadurai, R. Jose, Electrolyte selection for supercapacitive devices: A critical review, Nanoscale Adv. 1 (2019) 3807–3835. https://doi.org/10.1039/c9na00374f.

[44] H. Banda, S. Périé, B. Daffos, P.-L. Taberna, L. Dubois, O. Crosnier, P. Simon, D. Lee, G. De Paëpe, F. Duclairoir, Sparsely Pillared Graphene Materials for High-Performance Supercapacitors: Improving Ion Transport and Storage Capacity, ACS Nano 13 (2019) 1443–1453. https://doi.org/10.1021/acsnano.8b07102.

[45] F.W. Richey, B. Dyatkin, Y. Gogotsi, Y.A. Elabd, Ion Dynamics in Porous Carbon Electrodes in Supercapacitors Using in Situ Infrared Spectroelectrochemistry, J. Am. Chem. Soc. 135 (2013) 12818–12826. https://doi.org/10.1021/ja406120e.

[46] J. Chmiola, Anomalous Increase in Carbon Capacitance at Pore Sizes Less Than 1 Nanometer, Science 313 (2006) 1760–1763. https://doi.org/10.1126/science.1132195.

[47] Z. Xiong, T. Gu, X. Wang, Self-Assembled Multilayer Films of Sulfonated Graphene and Polystyrene-Based Diazonium Salt as Photo-Cross-Linkable Supercapacitor Electrodes, Langmuir 30 (2014) 522–532. https://doi.org/10.1021/la4037875.

[48] S. Alipour, S.M. Mousavi-Khoshdel, Investigation of the electrochemical behavior of functionalized graphene by nitrophenyl groups as a potential electrode for supercapacitors, Electrochim. Acta 317 (2019) 301–311. https://doi.org/10.1016/j.electacta.2019.05.029.

[49] Y. Zhuo, I.A. Kinloch, M.A. Bissett, Simultaneous Electrochemical Exfoliation and Chemical Functionalization of Graphene for Supercapacitor Electrodes, J. Electrochem. Soc. 167 (2020) 110531. https://doi.org/10.1149/1945-7111/aba3ff.

[50] D. Yang, C. Bock, Laser reduced graphene for supercapacitor applications, J. Power Sources. 337 (2017) 73–81. https://doi.org/10.1016/j.jpowsour.2016.10.108.

[51] M. Kang, D.H. Lee, Y.-M. Kang, H. Jung, Electron beam irradiation dose dependent physico-chemical and electrochemical properties of reduced graphene oxide for supercapacitor, Electrochim. Acta 184 (2015) 427–435. https://doi.org/10.1016/j.electacta.2015.10.053.

[52] M. Kota, X. Yu, S.-H. Yeon, H.-W. Cheong, H.S. Park, Ice-templated three dimensional nitrogen doped graphene for enhanced supercapacitor performance, J. Power Sources 303 (2016) 372–378. https://doi.org/10.1016/j.jpowsour.2015.11.006.

[53] Z. Wen, X. Wang, S. Mao, Z. Bo, H. Kim, S. Cui, G. Lu, X. Feng, J. Chen, Crumpled Nitrogen-Doped Graphene Nanosheets with Ultrahigh Pore Volume for High-Performance Supercapacitor, Adv. Mater. 24 (2012) 5610–5616. https://doi.org/10.1002/adma.201201920.

[54] K. Kakaei, M. Hamidi, S. Husseindoost, Chlorine-doped reduced graphene oxide nanosheets as an efficient and stable electrode for supercapacitor in acidic medium, J. Colloid Interface Sci. 479 (2016) 121–126. https://doi.org/10.1016/j.jcis.2016.06.058.

[55] K. Fujisawa, R. Cruz-Silva, K.-S. Yang, Y.A. Kim, T. Hayashi, M. Endo, M. Terrones, M.S. Dresselhaus, Importance of open, heteroatom-decorated edges in chemically doped-graphene for supercapacitor applications, J. Mater. Chem. A 2 (2014) 9532–9540. https://doi.org/10.1039/C4TA00936C.

[56] X. Ye, Y. Zhu, H. Jiang, L. Wang, P. Zhao, Z. Yue, Z. Wan, C. Jia, A rapid heat pressing strategy to prepare fluffy reduced graphene oxide films with meso/macropores for high-performance supercapacitors, Chem. Eng. J. 361 (2019) 1437–1450. https://doi.org/10.1016/j.cej.2018.10.187.

[57] H.-W. Chang, Y.-R. Lu, J.-L. Chen, C.-L. Chen, J.-M. Chen, Y.-C. Tsai, W.C. Chou, C.-L. Dong, Electrochemically Activated Reduced Graphene Oxide Used as Solid-State Symmetric Supercapacitor: An X-ray Absorption Spectroscopic Investigation, J. Phys. Chem. C 120 (2016) 22134–22141. https://doi.org/10.1021/acs.jpcc.6b04936.

[58] C. Shen, R. Li, L. Yan, Y. Shi, H. Guo, J. Zhang, Y. Lin, Z. Zhang, Y. Gong, L. Niu,

Rational design of activated carbon nitride materials for symmetric supercapacitor applications, Appl. Surf. Sci. 455 (2018) 841–848. https://doi.org/10.1016/j.apsusc.2018.06.065.

[59] S.S. Balaji, M. Karnan, J. Kamarsamam, M. Sathish, Synthesis of Boron-Doped Graphene by Supercritical Fluid Processing and its Application in Symmetric Supercapacitors using Various Electrolytes, ChemElectroChem. 6 (2019) 1492–1499. https://doi.org/10.1002/celc.201801490.

[60] S.S. Balaji, M. Karnan, P. Anandhaganesh, S.M. Tauquir, M. Sathish, Performance evaluation of B-doped graphene prepared via two different methods in symmetric supercapacitor using various electrolytes, Appl. Surf. Sci. 491 (2019) 560–569. https://doi.org/10.1016/j.apsusc.2019.06.151.

[61] S.S. Balaji, J. Anandha Raj, M. Karnan, M. Sathish, Supercritical fluid assisted synthesis of S-doped graphene and its symmetric supercapacitor performance evaluation using different electrolytes, Synth. Met. 255 (2019) 116111. https://doi.org/10.1016/j.synthmet.2019.116111.

[62] S.S. Balaji, M. Karnan, M. Sathish, Symmetric electrochemical supercapacitor performance evaluation of N-doped graphene prepared via supercritical fluid processing, J. Solid State Electrochem. 22 (2018) 3821–3832. https://doi.org/10.1007/s10008-018-4086-9.

Facile and mild covalent functionalization of rGO *via* aryne coupling

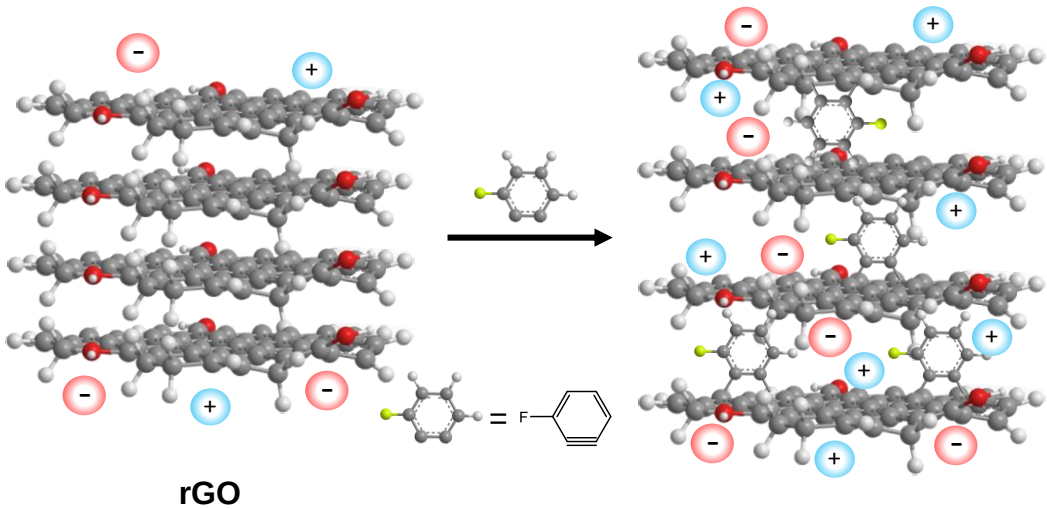

Two symmetric supercapacitors